The Journal of Chemical Physics

RESEARCH ARTICLE | NOVEMBER 07 2023

Spin singlet pairing of bismuth in titania

Jing Chang; Haoxiang Chen ; Peng Gao ; Ji Chen

J. Chem. Phys. 159, 174709 (2023)
https://doi.org/10.1063/5.0176355

AIP Publishing

The Journal of Chemical Physics ARTICLE pubs.aip.org/aip/jcp

Spin singlet pairing of bismuth in titania

Cite as: J. Chem. Phys. 159, 174709 (2023); doi: 10.1063/5.0176355
Submitted: 13 September 2023 • Accepted: 1 October 2023 •
Published Online: 7 November 2023

Jing Chang,[1] Haoxiang Chen,[2] Peng Gao,[1,3,4,a)] and Ji Chen[1,3,5,b)]

AFFILIATIONS

[1] School of Physics, Peking University, Beijing 100871, People's Republic of China
[2] Institute of Condensed Matter and Material Physics, School of Physics, Peking University, Beijing 100871, People's Republic of China
[3] Interdisciplinary Institute of Light-Element Quantum Materials and Research Center for Light-Element Advanced Materials, Peking University, Beijing 100871, People's Republic of China
[4] Collaborative Innovation Center of Quantum Matter, Beijing 100871, People's Republic of China
[5] Frontiers Science Center for Nano-Optoelectronics, Peking University, Beijing 100871, People's Republic of China

[a)] **Electronic mail:** p-gao@pku.edu.cn
[b)] **Author to whom correspondence should be addressed:** ji.chen@pku.edu.cn

ABSTRACT

The formation of electron and hole traps in semiconductors via atomistic defects is the fundamental microscopic mechanism for tuning the electronic and photonic properties of these materials. Here we find in experiments that bismuth atoms doped into anatase TiO_2 as substituents can appear as paired diatomic defects. Through first-principles density functional theory calculations, we reveal that the observed bismuth pair is separated by a medium distance of 6.37 Å through a delicate balance of Pauli repulsion and effective attractive interaction. We further clarify that the effective attractive interaction is related to the exchange coupling between the two bismuth defect states, which also leads to the formation of a spin singlet electronic state of the two unpaired electrons. Our study brings up a new type of defect state in TiO_2, and motivates further experimental and theoretical studies of multi-electronic states in materials.

I. INTRODUCTION

Titanium dioxide (TiO_2) has been widely studied for its promising photocatalytic behavior.[1,2] Pristine anatase TiO_2 is a semiconductor with a band gap of ~3.2 eV, within which defect states formed have attracted a large amount of research attention aimed at improving the photo-catalytic efficiency.[3–10] From the theoretical perspective, understanding the electronic states of these defects in TiO_2 has been a key challenge and thus motivates many studies.[11–15] Here we discuss one specific case, namely the Bi substituent in TiO_2. Existing works have focused mainly on materials engineering aimed at understanding the macroscopic efficiency, whereas microscopic details regarding e.g. the atomic structure and the electronic structure of Bi-doped TiO_2 are yet to explore.[16–18]

In TiO_2, excess electron doping is a rather general phenomenon, with other examples such as Ti interstitial, oxygen vacancy and photoelectrons.[1,3] These excess electrons may come from different sources, but they appear to have common features such as the formation of electronic polarons due to electron phonon couplings.[15,19] Beyond their common features, excess electrons may also have quite different states which are related to the nature of the dopants. The direct consequences of different electronic states are the different defect levels and different spin states associated with excess electrons.[20–22] For example, recent theoretical studies have clarified that the oxygen vacancy has a spin singlet state in TiO_2.[22] These works suggest that the electronic structure of Bi doping may also have some interesting features.

Here we report a joint experimental and theoretical study to understand the microscopic details of Bi doping pair in TiO_2. Atomic resolution scanning transmission electron microscopy (STEM) measurements identify the formation of pairs of Bi substituents in TiO_2. Density functional theory calculations further reveal that the atomic structure of Bi pair consists of two Bi atoms separated by 2.66 Å in the [010] direction, which is not resolved in STEM images. In addition, we find the most stable Bi pair has a unique spin singlet state, whereas other meta-stable Bi pairs all result in spin triplets. Our results suggest an interesting medium-range spin coupling indicating the exchange mechanism between two defect states that are not fully localized.

II. EXPERIMENTAL AND COMPUTATIONAL DETAILS

The TiO_2 were directly deposited on (001) pseudocubic $BiFeO_3$ by pulsed laser deposition. During the growth, the spontaneous diffusion of Bi atoms forms defects in TiO_2. Cross-sectional scanning transmission electron microscope specimens were thinned by mechanical polishing and followed by argon ion milling in a Precision Ion Polishing System 691 (Gatan). A typical ion milling procedure consists of two steps. In the first stage of coarse milling, the guns were at 4 keV with angles 5° and −5°. In the following condition, the guns were set at 1 keV for 5 min with angles of 3.5° and −3.5°, and further lowered to 0.2 keV for about one minute for final cleaning of the possible amorphous layer. High-angle annular dark field (HAADF) and annular bright field (ABF) images were simultaneously recorded at 300 kV in JEM ARM300CF (JEOL Ltd.). The convergence semi-angle for imaging is 24 mrad, collection semi-angles snap is 65–240 mrad for HAADF imaging and 12–24 mrad for ABF imaging.

Density functional theory calculations were carried out using the Vienna *Ab Initio* Simulation Package (VASP).[23,24] Projected augmented wave (PAW) method was used in conjunction with a 500 eV cutoff for plane wave expansion.[25,26] We have used Perdew–Burke–Ernzerhof (PBE),[27] PBE+U (valid U = 4.0 for 3d orbitals of Ti)[28,29] and HSE06[30,31] exchange-correlation functionals to calculate the energy, and used the HSE06 functional to calculate the electronic structure. HSE06 is a hybrid functional, which can well describe the band gap of TiO_2 and defect electronic structure. A $3 \times 2 \times 1$ supercell of anatase and a $2 \times 4 \times 4$ Monkhorst-Pack k-points[31] grid for the Brillouin zone integration were employed. Geometry optimizations were converged until residual forces on all ions were less than 0.02 eV/Å. The climbing image nudged elastic band (CI-NEB)[32] was used to determine the energy barriers of various kinetic processes. CI-NEB calculations were performed with the PBE exchange-correlation functional. The analyses of the electron hopping strength were carried out using the PySCF code.[33]

III. RESULTS AND DISCUSSIONS

A. Experimental observation of Bi pair in TiO_2

Bi doping is achieved in our experiments by preparing an interface between TiO_2 and $BiFeO_3$. Bi gradually diffuses from the interface to the regime of TiO_2. Figure 1 presents a typical atomic resolution STEM image of the sample along [001] direction of the anatase TiO_2 lattice, where the Bi-doped site features a brighter spot due to the Z-contrast nature of HAADF. The light blue dots highlight the Ti columns in TiO_2, which shows darker spots in the HAADF image. An interesting observation from the STEM image is that the doped Bi atoms tend to diffuse into paired dimers. Among hundreds of images collected in our experiments, such dimers appear in more than a dozen of images, which indicates that the paired dimer is thermodynamically stable. We further note that although in most of the experiments Bi-pairs are not observed, once the Bi dopants enter the TiO_2 lattice, Bi dimers are dominant,

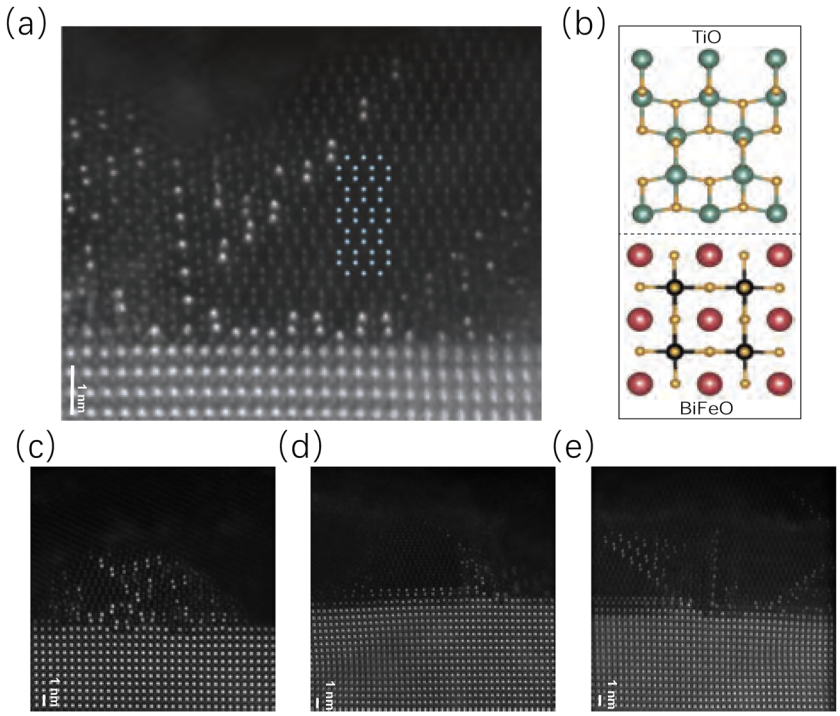

FIG. 1. Experimental atomic resolution STEM-HAADF image of the TiO_2–$BiFeO_3$ interface. (a) The brightest spots are Bi substituents, and the light blue dots indicate the pristine lattice of Ti. (b) The right panel is an illustration of the interface model, where the green, orange, red and black color represent the Ti, O, Bi, Fe atoms, respectively. (c)–(e) Three other experimental images showing Bi pairs.

which is a strong evidence of the pairing. More discussions about the thermodynamics stability and kinetic effects will be given in Secs. III C and III D. The observation of pairing suggests that there is a kind of attractive interaction between doped Bi atoms embedded in TiO_2 lattice. The interaction may also induce multi-electron states of the defect.

B. Single Bi substituent in TiO_2

To establish a clear theoretical understanding of the Bi defects, we shall first have in mind that Ti atom has four valence electrons, which would fully transfer to the 2p orbitals of O atoms in TiO_2, forming Ti^{4+} cations and O^{2-} ions. This leads to a valence band with O(2p) states and a conduction band with Ti(3d) states. Further, since Bi atom has five valence electrons outside the full 5d shell, including two 6s electrons and three 6p electrons, Bi naturally forms Bi_2O_3 and Bi_2O_5 oxides, in a Bi^{3+} and Bi^{5+} state, respectively. When a Bi atom is doped into TiO_2, the most favorable form is a substituent of Ti and it induces a hole doping or an electron doping, which can be seen from the following electronic structures of Bi substituent in TiO_2.

Before investigating Bi-pairs, as seen in Fig. 2, the structure of a single Bi substituent in TiO_2 and its electronic structure are first studied. After structure optimization with the HSE method, the lattice of Bi-doped TiO_2 displays a slight expansion due to the bigger radius of Bi than Ti. The parameters increase by about 0.3 and 0.6 Å in the [100] and [001] directions, respectively. The Bi–O bond length is about 2.2 Å, which is 0.2 Å longer than the Ti–O bond. The band gap of pure anatase TiO_2 is ~3.3 eV calculated with HSE. With substituent Bi atoms, the band gap remains largely unchanged. The substituent Bi atom induces extra gap states both above and under the Fermi level, as shown in the density of states (DOS) [Fig. 2(b)]. These gap states can act as electron and hole traps. From the zoom-in plot of DOS [Fig. 2(d)], it can be seen that the gap states are contributed by not only Bi(s) but also O(2p) and Ti(3d) electrons. One Bi dopant induces one electron in the defect, so one molecular orbital can split into two spin orbitals, where one is occupied and one is unoccupied. Figure 2(c) shows the partial charge density corresponding to the gap state, which also shows that the defect state is not localized on the Bi atom, but extends to a few shells of atoms.

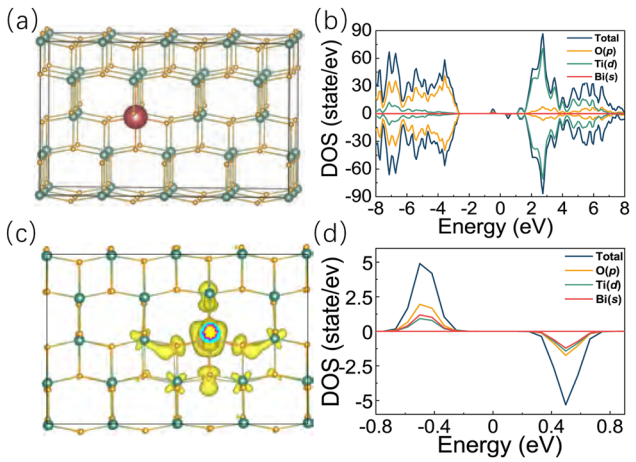

FIG. 2. The single Bi-doped anatase TiO_2. (a) Atomic structure of the supercell used in the calculation. Red, green and orange spheres are Bi, Ti and O atoms, respectively. (b) Total and partial density of states (DOS). (c) Partial charge density corresponds to the gap states. (d) Zoom-in of the DOS around Fermi level.

C. Thermodynamic stability of Bi pairs

Now we discuss the Bi pairs observed in experiments. The performed experimental image lacks information on the depth of Bi atoms, so the exact position and distance of the two Bi atoms can not be explicitly determined. To understand the thermodynamic stability of Bi dimers in TiO_2, we carry out a series of density functional theory (DFT) calculations, considering five possible dimer configurations. The configurations are shown in Fig. 3(a), from two different perspectives, and the right panel shows the perspective along the [001] direction corresponding to the experimental images. They are labeled as configuration I, II, III, IV, and V. Among the five structures, I and II can reproduce the experimental image of the Bi dimer.

The relative energy is calculated with three different methods and plotted in Fig. 3(b). With HSE exchange-correlation functional, configuration I is the most stable structure. Configurations II and III are two structures in that the distance between two Bi atoms is smaller than configuration I. However, their relative energies are 0.192 and 0.172 eV, respectively, and are less stable than configuration I. Bi atoms in configurations IV and V are farther away than configuration I, and their energies are also higher. We trust the HSE calculations to be reliable, but to further test the validity of our conclusion, we also carried out calculations using the PBE functional and PBE with an additional on-site interaction U. These test calculations show consistently that configuration I is the most stable.

The finding that configuration I is the most stable is interesting because it has a medium-range separation. When two Bi atoms approach each other, a repulsive interaction might occur due to Pauli repulsion, which can explain why configuration II and configuration III are less stable. The repulsive interaction can also be understood by comparing the behavior of other functionals. PBE functional yields much higher energy for configuration II, which is consistent with the fact that PBE underestimates the electron localization effects, leading to a larger overlap between the two Bi defects and stronger Pauli repulsion. In addition to the repulsion that becomes important for close pairs, our results suggest that there is also an attractive interaction between two Bi-atoms in configuration I, so that they also like to pair instead of separate. By comparing the energy of configuration I and that of configurations IV and V, we estimate that this effective interaction can be as large as 0.1 eV. In Sec. III E, we will see that this is related to the exchange interaction leading to spin anti-parallel alignment.

D. The diffusion kinetics of Bi atom in TiO_2 lattice

To further understand the formation kinetics of Bi pairs, we carried out CI-NEB calculations. Figures 4(a) and 4(b) shows the two considered transitions involving the interchange of a Bi and a near Ti atom, which can represent the two typical processes of Bi diffusion in the anatase lattice. For Bi diffusion along the [001] and [100] direction of anatase, it can either go through the first or the second transition pathway. For Bi diffusion along the [010] crystalline direction, only the first transition pathway is relevant.

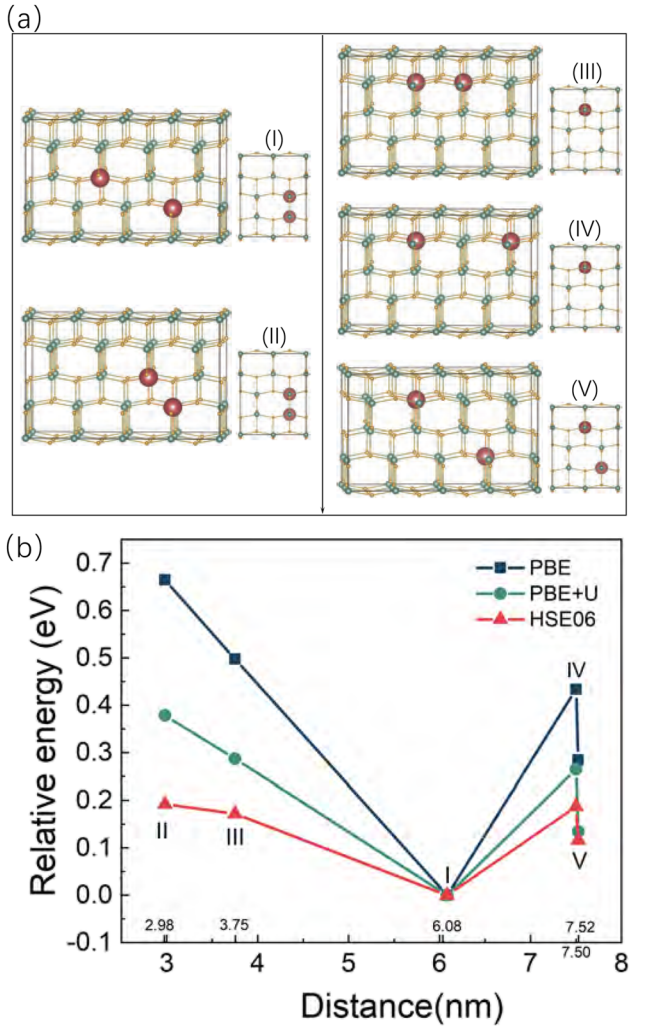

FIG. 3. Structures and stability of Bi pair in anatase TiO_2. (a) Five possible structural models, labeled from I to V. The left sub-panel is the perspective angle in the [100] direction, with the horizontal direction being [001]. The right sub-panel is the perspective angle in the [001] direction, which is the left-side view of the left sub-panel. (b) Relative energies of the five configurations as a function of Bi–Bi distance calculated using three different methods of DFT. The Bi–Bi distance is 2.98, 3.75, 6.08, 7.50, 7.52 Å, respectively.

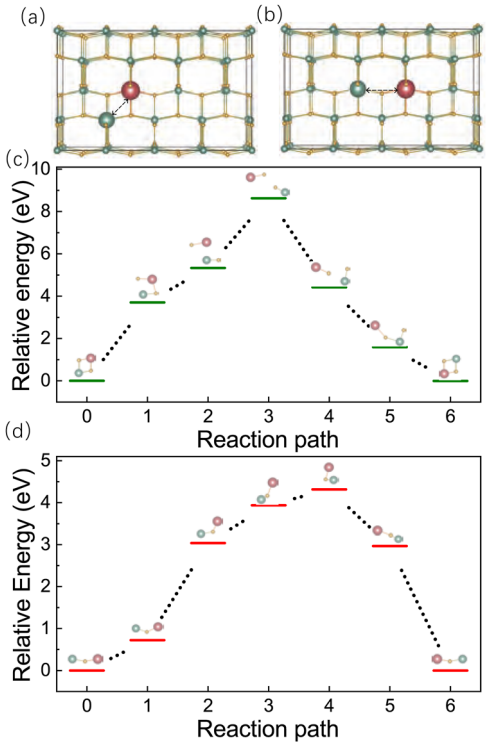

FIG. 4. The diffusion of Bi atom in TiO_2 lattice. (a) and (b) Illustration of the two diffusion paths, where a highlighted Bi atom swaps position with the nearest Ti atom. The red, green and yellow spheres represent the Bi, Ti and O atoms, respectively. (c) and (d) The CI-NEB computed reaction paths for the diffusion paths indicated in (a) and (b). The x-axis is the index of NEB image, the y-axis is the relative energy shown by the horizontal lines. Insets are snapshots showing the relative position of the swapping Ti–Bi pair and the connected O atoms during the transition.

The first transition pathway involves a Bi and a Ti atom forming a rhomboid with two connecting O atoms, and the second path swaps Bi with Ti along the [001] direction of TiO_2 anatase bridged by one O atom. Figures 4(c) and 4(d) shows the CI-NEB calculations for the two paths, respectively, including both the energies and the snapshots of the most relevant Ti, Bi and O atoms. For the first path, the Bi–O–O–Ti rhomboid first breaks as Bi and Ti atoms, and moves in two opposite directions. The movements are not in the line of the two atoms, but feature an effective rotation of the relative positions of the Bi and Ti atoms. In the initial configuration, the Bi–Ti distance is 3.10 Å, and the rotational movement allows the two cations to remain separated as much as possible to suppress the large cation–cation repulsion, even though the rotation causes significant lattice distortions around the defect. In Fig. 4, only the oxygen atoms within the initial rhomboid are shown, in which one moves alongside the Bi atom and the other is attached to the Ti atom. In such a manner, both the Bi atom and the Ti atom can form enough bonding with their nearest oxygen atoms despite that the bonds are also significantly distorted. At the transition state, the Bi–Ti distance is 2.68 Å, and the Ti and Bi atoms have moved to the original position of the two O atoms of the rhomboid. The transition state structure features the largest lattice distortion. After crossing the transition state, as the Ti and Bi atoms move towards their interchanged positions, the original anatase lattice gradually recovers.

In the second transition, the Bi atom moves mostly towards the Ti site, in the up-left direction in the shown figure. Simultaneously, the Ti atom moves away downward first and then right to the transition state. After passing the transition state, the Bi atom moves in the down-left direction and the Ti atom moves in the up-right direction toward their interchanged positions. During the transition, the original coordination of both cations and the positions of oxygen atoms around them also change significantly due to large structural distortions, which also recover when reaching the final state.

Comparing the two transition pathways, we find the second pathway has a lower barrier of about 4.3 eV, and the first pathway is about 8.6 eV. First of all, both barriers are quite large, which explains why the formed Bi defects are quite stable during the imaging experiments. The observation that only a few Bi atoms are observed to diffuse into the anatase lattice from the interface during the preparation of the sample can also be explained by the large diffusion barriers calculated. In addition, the much higher barrier of the first pathway means that the diffusion along the [010] lattice direction is suppressed, so that it can also inhibit the diffusion of Bi in the normal direction of the interface.

The interface might also affect the experimental observation. To this end, we have computed the diffusion barrier of Bi across the $BiFeO_3/TiO_2$ interface. We have tried several possible interfacial structures, and the lowest transition barrier is 9.5 eV, as indicated in Fig. S2. The barrier is even larger than the diffusion barrier of Bi in the TiO_2 lattice, which means that the rate-limiting step of Bi-doping is likely to be the step of Bi entering the TiO_2 lattice. The calculations also agree with the fact that Bi-pair is not observed in many experimental samples.

E. Defect electronic state

To understand the stable medium-range Bi pair we further investigate the electronic structure. Figure 5 shows the calculated density of states (DOS) of the five possible configurations using HSE functional. As can be seen, different configurations of Bi pair have very different electronic states. Similar to the single Bi defect, the electronic states of Bi pair defects consist of the 6s states of Bi, 2p states of O and 3d states of Ti, shown by the projected DOS. Figure 5(f) further plots the summary of the spin orbital levels for the five configurations with respect to their Fermi level. The electron/hole occupations of the spin states for the five configurations are also indicated with arrows. For configuration I, there is only

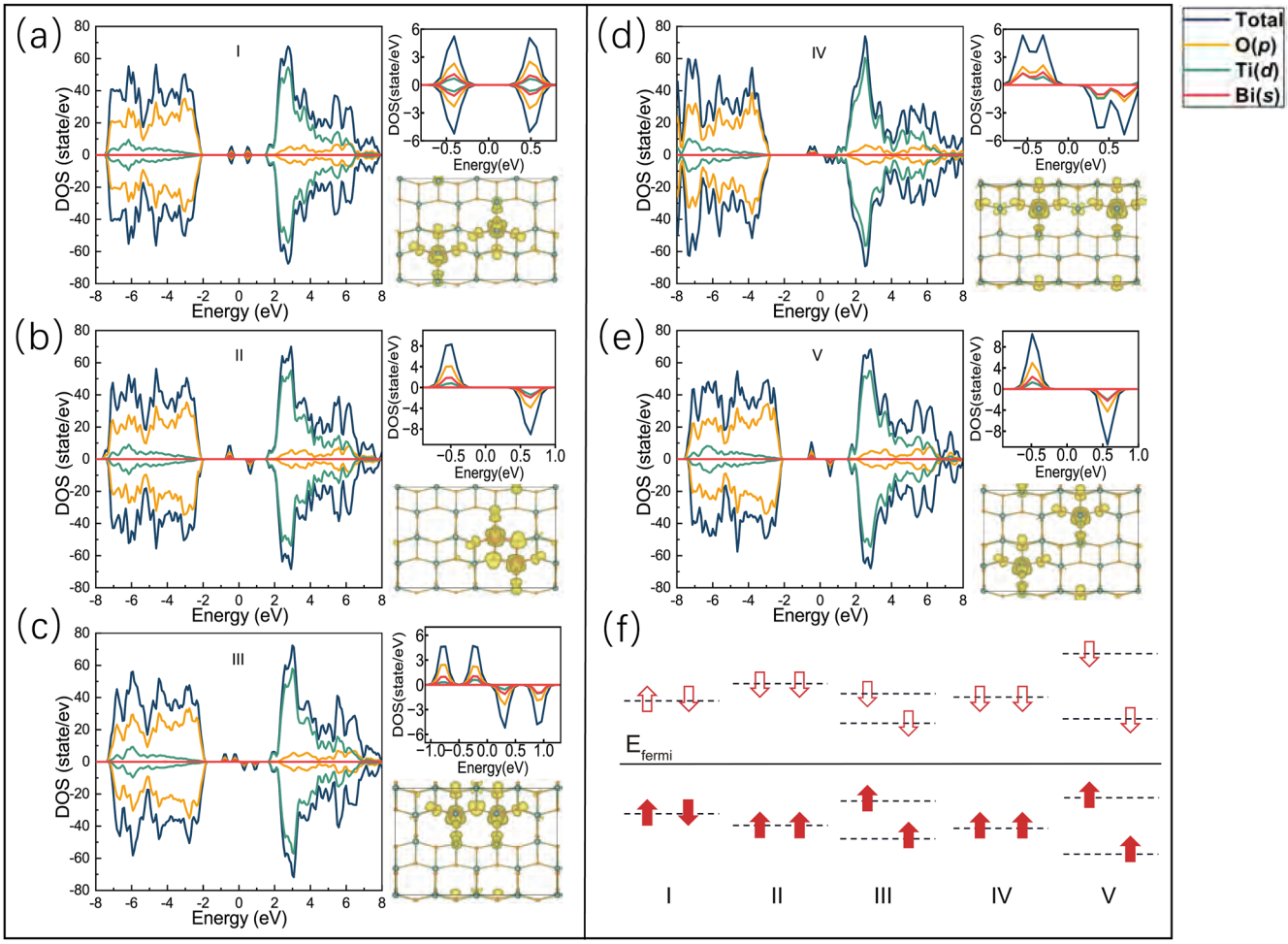

FIG. 5. Electronic structure of Bi pairs in five different configurations corresponding to Fig. 3. In each sub-panel, the left is the total and projected DOS, the right top is a zoom-in of the DOS around the gap states, and the right bottom is the partial charge density corresponding to the gap states. The iso-surface value to plot the partial charge density is 0.004 electrons/Å^3.

one level below the Fermi level, which hosts two electrons with the opposite spin. This shows the two electrons form a spin singlet state. On the contrary, for all other four configurations, the two electrons would feature the same spin polarization, occupying two spin orbitals that are not exactly at the same level and form triplet states. This suggests the formation of spin singlet state is related to the pairing of Bi in TiO_2 lattice.

Partial charge densities corresponding to the defect states are plotted in Fig. 5, and the spin coupling are further analyzed. Without considering exchange coupling, we assume the energy to be the same for different defect configurations. The energy of different configurations can be understand through spin coupling between defect states. For configuration I, the spin singlet state suggests that there is an interesting anti-ferromagnetic coupling, thus lowering the energy. We will discuss the exchange coupling mechanism in detail in Subsection III F. For configurations II and III, the two nearest neighbor defect centers are close, and they share the two oxygen atoms in the first neighborhood of Bi. As we have mentioned above, the first shell of the oxygen atom contributes significantly to the defect electronic state, there is a significant overlap between the two defects as shown by the partial charge density. The overlap of electron clouds increases Pauli repulsion and raises the energy of such configurations. For configuration IV, the defects are separated further apart by sharing a corner Ti atom. Ti(d) orbitals also contribute to defect states, but the contribution is much less. Therefore, the electron cloud overlap is less significant in configuration IV. For configuration V, the distance between two defects is largest in our model, and the coupling is weakest.

F. Exchange mechanisms

In anti-ferromagnetic materials, anti-parallel alignment of spins are typically induced via exchange mechanisms such as direct exchange, double-exchange, and super-exchange mechanisms. Direct exchange is a result of the direct electron hopping between nearest neighbor sites (Fig. 6). In our case although the two Bi sites are not adjacent to each other, their localized defect orbitals as a whole are in direct contact [Fig. 5(a)]. Therefore, the direct exchange mechanism is important. We can estimate the direct hopping strength (t_d) by computing the overlap integral of the two O(2p) atomic orbitals belonging to the two closest O atoms. The overlap is evaluated with an expansion towards atomic orbitals, and the direct hopping strength is estimated to be $t_d = 2.2$ eV (see supplementary material).

The super-exchange mechanism describes that two such localized orbitals are bridged via a doubly occupied p-orbital in an end-to-end orientation in transition metal oxides. The double-exchange mechanism can lead to both the ferromagnetic and the anti-ferromagnetic coupling in different circumstances. Here, the defect orbitals are mostly on the Bi and O atoms, and the possible bridging sites are the two Ti atoms connecting the O atoms. However, the Ti(3d) orbitals on the bridging Ti sites are all unoccupied, hence the standard super-exchange and the double exchange mechanisms are both forbidden in our case.

Nevertheless, we can still consider the two Ti atoms bridging the two O atoms as the leading contributors of the exchange mechanism. As Ti(3d) orbitals are higher in energy than defect orbitals, the electrons mainly reside on defect orbitals. Electrons can hop to bridging Ti, and then hop again to another defect orbital. Thus, effective hopping exists for defect orbitals with this "Ti-mediated" mechanism. We estimate that hopping strength between the defect-frontier O(2p) orbital and the bridging Ti(3d) orbital is $t_s = 2.7$ eV, with overlap integral similar to the case of direct mechanism. From the DOS calculation of Fig. 5, we also estimate that the energy gap between the defect orbital and the bridging Ti(3d) orbital is on the order of $E_{\mathrm{Ti}} = 1$ eV. Therefore, t_d is comparable to t_s^2/E_{Ti}, and the

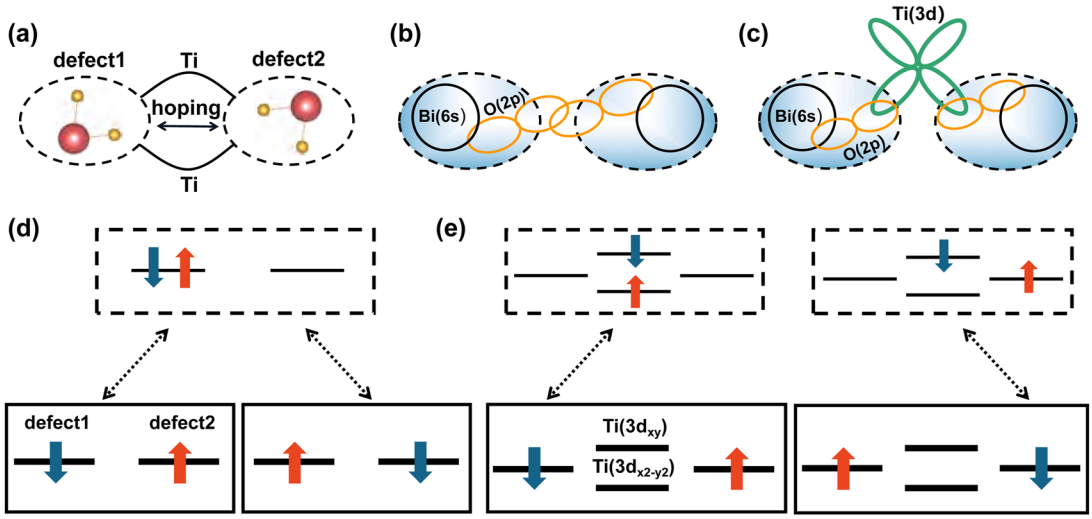

FIG. 6. Schematics for exchange mechanisms. (a) A schematic of the defect center and hoping model for the Bi pair in configuration I. (b) The orbital overlap for the direct exchange mechanism. (c) The orbital overlap for the "Ti-mediated" exchange mechanism. (d) and (e) show the spin occupation on orbitals of the direct exchange mechanism and "Ti-mediated" exchange mechanism. The black straight lines represent the spin orbitals, and different arrow represent the spin orientation. The antiparallel spins exchange with each other via effective high energy process as shown in the dashed boxes.

strength of this exchange mechanism is likely to comparable to the strength of the direct exchange, and should be consider relevant for anti-ferromagnetic coupling.

In a brief summary, here, we demonstrate that in the d^0 transition metal oxide TiO_2, the anti-parallel coupling can be induced by both direct (direct exchange mechanism) and effective (Ti-mediated mechanism) hopping between two defect sites, with the defect states not heavily localized on defect sites.

IV. CONCLUSIONS

To conclude, our study has revealed the formation of a new type of defect in TiO_2 lattice by atomically resolved STEM measurement and first-principles calculations. The defect is formed by a pair of bismuth atoms, which displays an interesting medium-range coupling due to the formation of a spin singlet state. The novel spin singlet state suggests the existence of anti-ferromagnetic coupling in such systems, extending our current understanding of exchange interactions in oxide materials, which is likely to lead to the exploration of novel magnetic structures in the future. It is worth noting that for complex magnetic structure with multiple magnetic sites, couplings beyond two-body may play important roles, hence understanding the pairing is the first step toward Bi doping in TiO_2 lattice. From a computational point of view, employing a larger supercell and systematically calculating different doping configurations can break down the electronic correlation effects into different types of couplings. In addition, the spin state formed by the Bi pair may play an important role in the photo-catalysis process with TiO_2 substrate.

SUPPLEMENTARY MATERIAL

The supplementary material contains additional experimental results, extended theoretical discussions on the exchange mechanism and the estimation of coupling parameters.

ACKNOWLEDGMENTS

This work was supported by the National Natural Science Foundation of China under Grant No. 92165101, the National Key R&D Program of China under Grant No. 2021YFA1400500, and the Strategic Priority Research Program of Chinese Academy of Sciences under Grant No. XDB33000000. J.C. is grateful for the support of the Beijing Natural Science Foundation (Grant No. JQ22001). We are grateful for computational resources supported by High-performance Computing Platform of Peking University, the TianHe-1A supercomputer and Shanghai Supercomputer Center. P.G. acknowledges Professor Ying-Hao Chu at National Chiao Tung University in Taiwan for providing the samples, and Professor Yuichi Ikuhara at The University of Tokyo for the use of electron microscope. The authors thank Ruixue Zhu for helpful discussions on experimental images.

AUTHOR DECLARATIONS

Conflict of Interest

The authors have no conflicts to disclose.

Author Contributions

J.C. and H.C. contributed equally to this work.

Jing Chang: Formal analysis (equal); Investigation (equal); Validation (equal); Visualization (equal); Writing – original draft (lead); Writing – review & editing (equal). **Haoxiang Chen**: Formal analysis (equal); Investigation (equal); Validation (equal); Visualization (equal); Writing – review & editing (equal). **Peng Gao**: Data curation (equal); Formal analysis (equal); Investigation (equal); Validation (equal); Writing – review & editing (supporting). **Ji Chen**: Conceptualization (lead); Formal analysis (equal); Funding acquisition (lead); Resources (lead); Supervision (lead); Writing – original draft (lead); Writing – review & editing (lead).

DATA AVAILABILITY

The data that support the findings of this study are available from the corresponding author upon reasonable request.

REFERENCES

[1] T. L. Thompson and J. T. Yates, "Surface science studies of the photoactivation of TiO_2-new photochemical processes," Chem. Rev. **106**, 4428–4453 (2006).
[2] A. Fujishima, X. Zhang, and D. A. Tryk, "TiO_2 photocatalysis and related surface phenomena," Surf. Sci. Rep. **63**, 515–582 (2008).
[3] S. Wendt, P. T. Sprunger, E. Lira, G. K. H. Madsen, Z. Li, J. Hansen, J. Matthiesen, A. Blekinge-Rasmussen, E. Lægsgaard, B. Hammer, and F. Besenbacher, "The role of interstitial sites in the Ti3*d* defect state in the band gap of Titania," Science **320**, 1755–1759 (2008).
[4] R. Long and N. J. English, "Synergistic effects of Bi/S codoping on visible light-activated anatase TiO_2 photocatalysts from first principles," J. Phys. Chem. C **113**, 8373–8377 (2009).
[5] M. A. Henderson, "A surface science perspective on TiO_2 photocatalysis," Surf. Sci. Rep. **66**, 185–297 (2011).
[6] C. L. Pang, R. Lindsay, and G. Thornton, "Structure of clean and adsorbate-covered single-crystal rutile TiO_2 surfaces," Chem. Rev. **113**, 3887–3948 (2013).
[7] S. Selcuk and A. Selloni, "Facet-dependent trapping and dynamics of excess electrons at anatase TiO_2 surfaces and aqueous interfaces," Nat. Mater. **15**, 1107–1112 (2016).
[8] M. Reticcioli, I. Sokolović, M. Schmid, U. Diebold, M. Setvin, and C. Franchini, "Interplay between adsorbates and polarons: CO on rutile TiO_2(110)," Phys. Rev. Lett. **122**, 016805 (2019).
[9] J. Chang, Z.-Y. Jiang, Z.-Y. Zhang, Y.-M. Lin, P.-L. Tian, B. Zhou, and L. Chen, "Theoretical studies of photocatalytic behaviors of isoelectronic C/Si/Ge/Sn-doped TiO_2: DFT+U," Appl. Surf. Sci. **484**, 1304–1309 (2019).
[10] L. Zhang, W. Chu, Q. Zheng, and J. Zhao, "Effects of oxygen vacancies on the photoexcited carrier lifetime in rutile TiO_2," Phys. Chem. Chem. Phys. **24**, 4743–4750 (2022).
[11] N. A. Deskins and M. Dupuis, "Electron transport via polaron hopping in bulk TiO_2: A density functional theory characterization," Phys. Rev. B **75**, 195212 (2007).
[12] P. Deák, B. Aradi, and T. Frauenheim, "Quantitative theory of the oxygen vacancy and carrier self-trapping in bulk TiO_2," Phys. Rev. B **86**, 195206 (2012).
[13] A. Janotti, C. Franchini, J. B. Varley, G. Kresse, and C. G. Van de Walle, "Dual behavior of excess electrons in rutile TiO_2," Phys. Status Solidi RRL **7**, 199–203 (2013).
[14] C. Guo, X. Meng, H. Fu, Q. Wang, H. Wang, Y. Tian, J. Peng, R. Ma, Y. Weng, S. Meng, E. Wang, and Y. Jiang, "Probing nonequilibrium dynamics of photoexcited polarons on a metal-oxide surface with atomic precision," Phys. Rev. Lett. **124**, 206801 (2020).
[15] C. Franchini, M. Reticcioli, M. Setvin, and U. Diebold, "Polarons in materials," Nat. Rev. Mater. **6**, 560 (2021).

[16]G. D. Bhowmick, M. T. Noori, I. Das, B. Neethu, M. M. Ghangrekar, and A. Mitra, "Bismuth doped TiO_2 as an excellent photocathode catalyst to enhance the performance of microbial fuel cell," Int. J. Hydrogen Energy **43**, 7501–7510 (2018).
[17]M.-C. Wu, J.-S. Chih, and W.-K. Huang, "Bismuth doping effect on TiO_2 nanofibres for morphological change and photocatalytic performance," CrystEngComm **16**, 10692–10699 (2014).
[18]J. H. Lee, H. Lee, and M. Kang, "Remarkable photoconversion of carbon dioxide into methane using Bi-doped TiO_2 nanoparticles prepared by a conventional sol-gel method," Mater. Lett. **178**, 316–319 (2016).
[19]J. Chen, C. Penschke, A. Alavi, and A. Michaelides, "Small polarons and the Janus nature of TiO_2(110)," Phys. Rev. B **101**, 115402 (2020).
[20]A. Janotti, J. B. Varley, P. Rinke, N. Umezawa, G. Kresse, and C. G. Van de Walle, "Hybrid functional studies of the oxygen vacancy in TiO_2," Phys. Rev. B **81**, 085212 (2010).
[21]A. Malashevich, M. Jain, and S. G. Louie, "First-principles DFT+*GW* study of oxygen vacancies in rutile TiO_2," Phys. Rev. B **89**, 075205 (2014).
[22]J. Chen, N. A. Bogdanov, D. Usvyat, W. Fang, A. Michaelides, and A. Alavi, "The color center singlet state of oxygen vacancies in TiO_2," J. Chem. Phys. **153**, 204704 (2020).
[23]G. Kresse and J. Furthmüller, "Efficient iterative schemes for *ab initio* total-energy calculations using a plane-wave basis set," Phys. Rev. B **54**, 11169–11186 (1996).
[24]G. Kresse and J. Hafner, "*Ab initio* molecular dynamics for open-shell transition metals," Phys. Rev. B **48**, 13115–13118 (1993).
[25]P. E. Blöchl, "Projector augmented-wave method," Phys. Rev. B **50**, 17953–17979 (1994).
[26]G. Kresse and D. Joubert, "From ultrasoft pseudopotentials to the projector augmented-wave method," Phys. Rev. B **59**, 1758–1775 (1999).
[27]J. P. Perdew, K. Burke, and M. Ernzerhof, "Generalized gradient approximation made simple," Phys. Rev. Lett. **77**, 3865–3868 (1996).
[28]M. H. Samat, A. M. M. Ali, M. F. M. Taib, O. H. Hassan, and M. Z. A. Yahya, "Hubbard U calculations on optical properties of 3*d* transition metal oxide TiO_2," Results Phys., **6**, 891–896 (2016).
[29]W. Chen, P. Yuan, S. Zhang, Q. Sun, E. Liang, and Y. Jia, "Electronic properties of anatase TiO_2 doped by lanthanides: A DFT+U study," Physica B **407**, 1038–1043 (2012).
[30]J. Heyd, G. E. Scuseria, and M. Ernzerhof, "Hybrid functionals based on a screened Coulomb potential," J. Chem. Phys. **118**, 8207–8215 (2003).
[31]P. E. Blöchl, O. Jepsen, and O. K. Andersen, "Improved tetrahedron method for Brillouin-zone integrations," Phys. Rev. B **49**, 16223–16233 (1994).
[32]G. Henkelman, B. P. Uberuaga, and H. Jónsson, "A climbing image nudged elastic band method for finding saddle points and minimum energy paths," J. Chem. Phys. **113**, 9901–9904 (2000).
[33]Q. Sun, T. C. Berkelbach, N. S. Blunt, G. H. Booth, S. Guo, Z. Li, J. Liu, J. McClain, S. Sharma, S. Wouters, and G. K.-L. Chan, "P_ySCF: The Python-based simulations of chemistry framework," WIREs Comput. Mol. Sci. **8**, 1340 (2018).